Hyperfine Interact (2017) 238:59
DOI 10.1007/s10751-017-1429-3

# Synthesis and characterization of $\alpha Fe_{2-x}M_xO_3$ (M = Co, Ni, Cu or Zn) photocatalysts for the degradation of the indigo carmine dye in water

**Edilailsa Januário de Melo[1] · João Paulo de Mesquita[1] · Márcio César Pereira[2] · Luis Carlos Duarte Cavalcante[3,4] · Edivaldo dos Santos Filho[1] · José Domingos Fabris[1,4] · José Domingos Ardisson[5] · Luiz Carlos Alves de Oliveira[4]**



**Abstract** If suitably prepared, hematite ($\alpha Fe_2O_3$)-based materials may be effective photocatalysts under visible light. Doping hematite with cations is assumed to improve the chemical photocatalyst performance of hematite. To check for these effects, the catalytic efficiency under visible radiation of the pure, Co-, Ni-, Cu-, or Zn-doped nanosized hematite samples was tested on the degradation of the indigo carmine dye, as a model molecule to simulate a generic organic substrate. These semiconductors with photocatalyst activity were first characterized by powder X-ray diffractometry, Mössbauer spectroscopy, scanning electron microscopy coupled with energy dispersive X-ray spectrometer, diffuse reflectance spectroscopy and by energy dispersive X-ray fluorescence. The most efficient photocalysts for the indigo carmine dye degradation were the Cu- and Zn-doped hematite samples. The relatively higher photocatalytic activity of these two samples are interpreted as being due to their relatively higher ability, among the tested semiconductors, to absorb the visible light, efficient charge separation and $e^-$-transference.

This article is part of the Topical Collection on *Proceedings of the 15th Latin American Conference on the Applications of the Mössbauer Effect (LACAME 2016), 13-18 November 2016, Panama City, Panama*
Edited by Juan A. Jaén

✉ José Domingos Fabris
jdfabris@ufmg.br

[1] Federal University of the Jequitinhonha and Mucuri Valleys (UFVJM), Campus JK, 39100-000 Diamantina, Minas Gerais, Brazil

[2] Institute of Science, Engineering, and Technology, Federal University of the Jequitinhonha and Mucuri Valleys (UFVJM), Campus Mucuri, 39803-371 Teófilo Otoni, Minas Gerais, Brazil

[3] Center of Natural Sciences, Federal University of Piauí (UFPI), 64049-550 Teresina, Piauí, Brazil

[4] Department of Chemistry, Federal University of Minas Gerais (UFMG), 31270-901 Belo Horizonte, Minas Gerais, Brazil

[5] Center for the Development of the Nuclear Technology (CDTN), 31270-901 Belo Horizonte, Minas Gerais, Brazil

Published online: 27 June 2017

**Keywords** Photocatalyst · Hematite · Indigo carmine dye

## 1 Introduction

The pollution of the natural water bodies has been very often related to the growing industrial and agricultural activities in the global scale. The efforts to reduce any harmful emission and to stimulate the production of cleaner energy sources have progressively addressed research issues towards the technological development of new catalysts also destined to remediate polluted natural environments [1, 2], very particularly water bodies.

Semiconductors that are based on metal cation oxides have been reportedly tested as photocatalysts in the degradation of organic and inorganic pollutants in water [3]. Hematite ($\alpha Fe_2O_3$) is thought to be a promising photocatalyst under visible light, taking into account its optical bandgap energy, chemical stability, low-cost, and natural abundance of the oxide or its precursors [1]. However, further development of such solid photocatalysts requires some drawbacks to overcome, as, for instance, its low conductivity and relatively fast recombination of electron-hole pairs [4, 5]. Obtaining suitable cation-doped semiconductors has been an effective challenge, in order to improve the chemical performance of photocatalysts that are based on hematite [6].

It is reported the preparation of nanosized cation-doped hematite samples ($\alpha Fe_{2-x}M_xO_3$; $M = Co^{2+}$, $Ni^{2+}$, $Cu^{2+}$ or $Zn^{2+}$) chemically synthesized *via* the co-precipitation method. Their physical, chemical and structural characterizations were assessed by several methods. It was evaluated the chemical effect of the dopants on the photocatalytic activity of the cation-doped hematite samples towards the degradation of the indigo carmine dye, which was used as a model molecule to simulate a generic organic substrate in water.

## 2 Experimental

### 2.1 Synthesis

The pure and cation-doped hematite samples were prepared as described in ref. [7]. In brief, 30 mL of 1 mol $L^{-1}$ NaOH and 5 mL of 1 mol $L^{-1}$ $NaHCO_3$ were added to 50 mL of 0.28 mol $L^{-1}$ $Fe(NO_3)_3.9H_2O$ at 90 ºC. Varied amounts of $CoCl_2.6H_2O$, $Ni(NO_3)_2.6H_2O$, $CuCl_2.2H_2O$ and $ZnCl_2$, all of them corresponding to 2 mass% of the metal cation, relatively to the iron mass in each case, were then added to the mixture. The new mixture was refluxed under stirring for 3 days at 90 ºC. The obtained solid was then dried at 50 ºC in an oven for 24 h.

### 2.2 Characterization

The X-ray fluorescence analysis of the samples was made with an energy dispersive X-ray fluorescence spectrometer Shimadzu EDX-720, with rhodium tube and silicon-lithium detector. Data were collected without vacuum, with the collimator set at 10 mm.

Scanning electron microscopy (SEM) images and energy dispersive X-ray spectroscopy (EDS) data for the synthesized pure and cation-doped hematite samples were obtained in an equipment Zeiss (FEG-SEM) model Sigma VP.

The Mössbauer spectra were collected at 298 K and 80 K in a constant acceleration transmission setup mode with a ~20 mCi $^{57}$Co/Rh-gamma-ray source. Data were stored in

a 512-channel MCS memory unit, with Doppler velocities ranging between approximately ±11 mm $s^{-1}$. Mössbauer isomer shifts are quoted relatively to the $\alpha$-Fe foil at room temperature. The experimental data were least squares fitted with Lorentzian-shaped resonance lines, by using the NORMOS™-90 computer program.

The powder X-ray diffraction (XRD) patterns were collected in an equipment Rigaku model D/Max Ultima Plus set to a current of 30 mA and a voltage of 40 kV, with the CuK$\alpha$ ($\lambda = 1.541838$ Å) radiation, at a scan rate of 1° $2\theta$ $min^{-1}$, from 20° to 80° $2\theta$. Silicon was used as an external standard. The average particle sizes (estimated as being the dimension of mean coherent length) for all these samples were calculated from the XRD data using the Scherrer equation [8] for the width at half-height corresponding to the (104) reflection peak, for each sample. The corresponding crystalline structures and unit cell volume were refined by the Rietveld technique using FULLPROF® 98 computer program.

The UV-vis diffuse reflectance spectrum was taken on dry, ground powders using a Varian Cary 5 spectrophotometer equipped with a diffuse reflectance accessory. $BaSO_4$ powder was used as a standard reference (100% transmission). The Tauc plot was used to estimate the bandgap energies.

### 2.3 Photocatalytic activity under visible light irradiation

The chemical photocatalytic activity was evaluated according to the decomposition of indigo carmine dye at 320 K in a batch photoreactor. Typically, 0.01 g of the solid photocatalyst was suspended into 30 mL of an aqueous solution containing indigo carmine dye 25 mg $L^{-1}$ and 25 µL of hydrogen peroxide 35 mass%. The photocatalytic tests were also carried out under the same conditions but with the aqueous medium free of the photocatalyst, in order to evaluate the photocatalytic activity of the sole $H_2O_2$. All measurements were made with a UV–vis spectrometer Varian model Cary 50 under a radiation $\geq$ 400 nm emitted from a LED lamp (12 W). The most suitable wavelength was selected by sweeping over the whole visible spectral range (Fig. 1). The light absorption of the indigo carmine dye aqueous solution was thus spectrophotometrically monitored at 610 nm, during the photodegradation reaction.

## 3 Results and discussion

### 3.1 Characterization of the solid photocatalysts

The SEM images and EDS patterns are shown in Fig. 2. The images reveal similar morphologies for all the samples. The EDS data clearly evidence the occurrence of the doping elements (Fig. 2) in selected grains of these samples. Si and eventually Na appear only from point probing certain grains probably due to some contamination for using NaOH in the Pyrex™glassware, for the chemical synthesis.

The results of the elemental chemical composition as determined by EDXRF showed that the relative contents of iron and of the metal cations in the Co-, Ni-, Cu-, or Zn-doped hematite samples are, respectively, 99.01(2) and 0.99(1) mass%; 96.82(1) and 3.18(5) mass%; 97.41(2) and 2.59(3) mass% and 97.92(2) and 2.08(3) mass%, respectively.

The XRD patterns for the corresponding samples are shown in Fig. 3a. They all exhibit characteristic reflection peaks that confirm the samples as being crystallized in the trigonal hexagonal structure of $\alpha Fe_2O_3$ (JCPDS card # 33-664 [9]) without any extra crystallographic phase that could eventually be derived from the dopants only. Figure 3b shows the

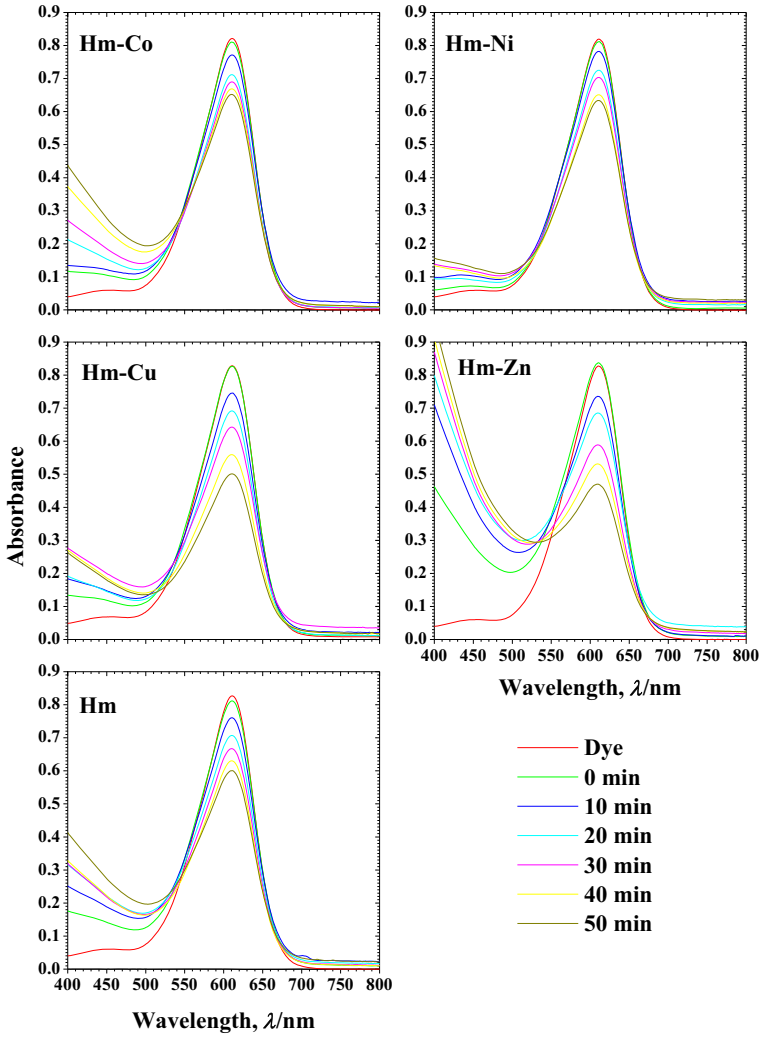


**Fig. 1** UV-vis spectra of indigo carmine dye during photocatalysis

expansion of the $2\theta$-scale between $20^{o}$ and $30^{o}$ to evidence the displacement of the (104) reflection peak according to the cation doping. The (104) peak position for the hematites was shifted to lower angle relatively to that for the pure hematite. This is a clear indication that the metal cations are successfully doped into the lattice of the $\alpha Fe_2O_3$ crystallographic structure.

The average particle sizes for all the samples as calculated from XRD data using the Scherrer equation are of 25.51 (Hm), 24.07 (Hm-Co), 21.25 (Hm-Ni), 25.40 (Hm-Cu) and 21.40 nm (Hm-Zn).

The optical bandgap value for hematite, determined from the Tauc plot from the UV-vis spectra, was estimated as being $\sim$1.92 eV. This result is in agreement with elsewhere reported estimations [10, 11]. For the nanosized Co-, Ni-, Cu-, or Zn-doped hematites, the

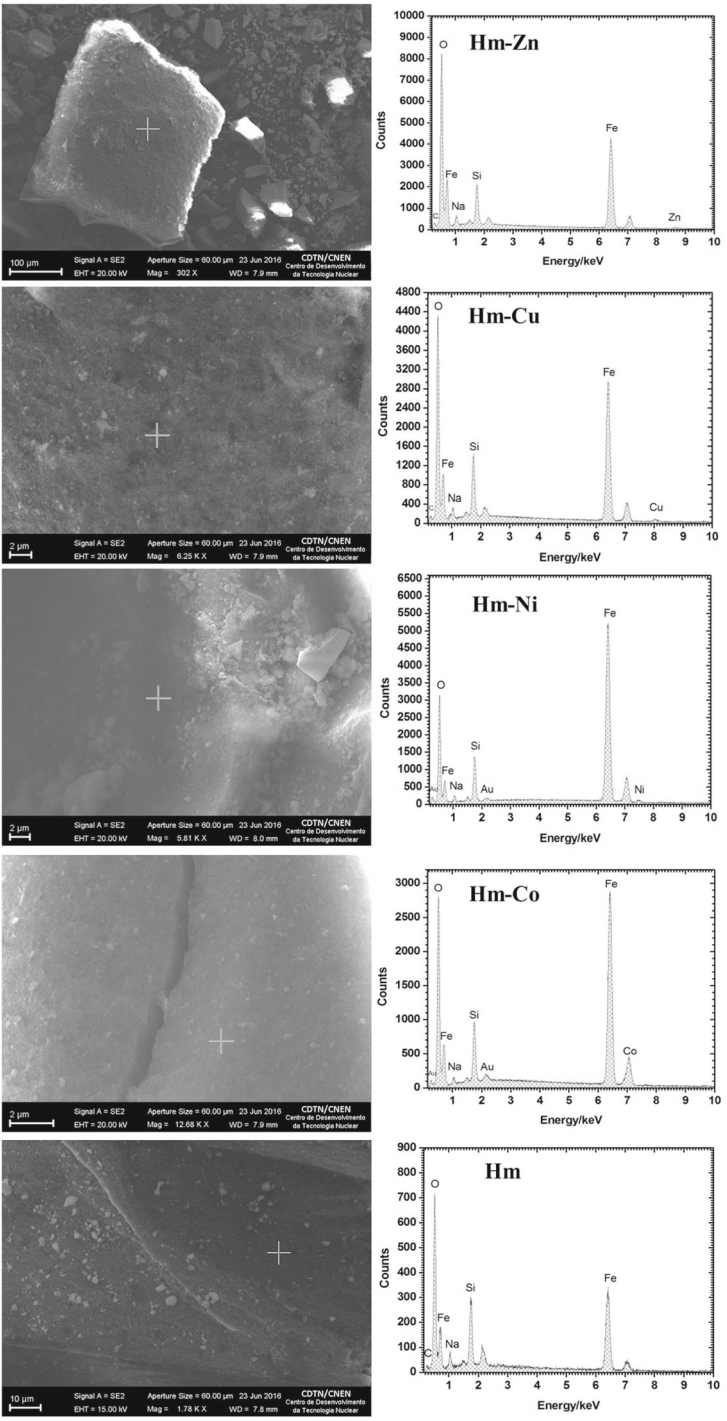


**Fig. 2** SEM images of the synthesized pure (Hm) and cation-doped hematite (Hm-Co to Hm-Zn) samples and corresponding EDS spectra for the point-probing selected particles

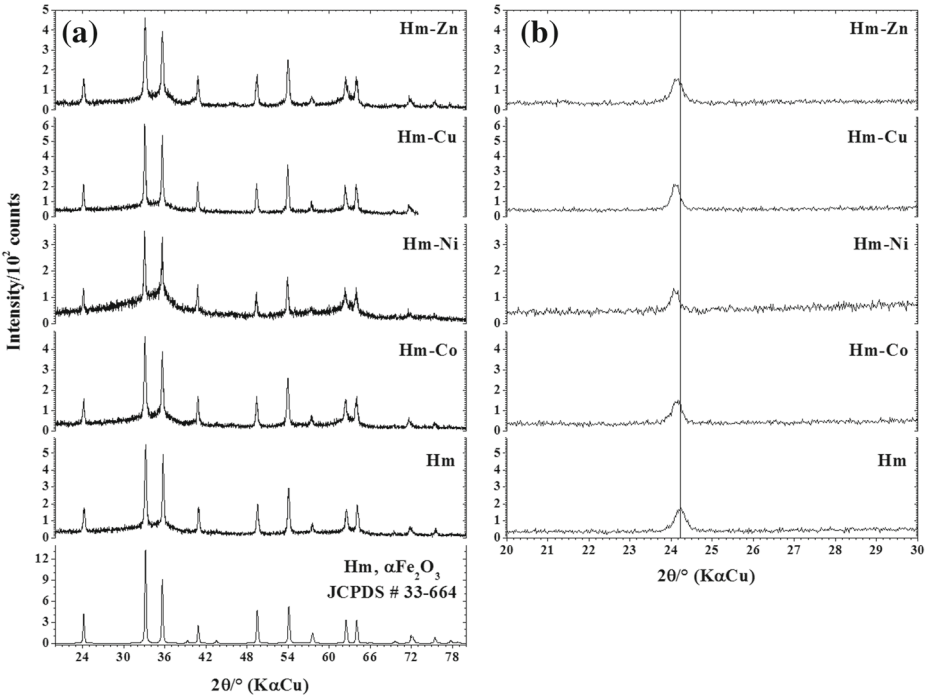


**Fig. 3** **a** Powder XRD patterns and (**b**) the magnification of the $2\theta$-scale between 20º and 30º to show the displacement of (012) reflection peak according to the doping cation

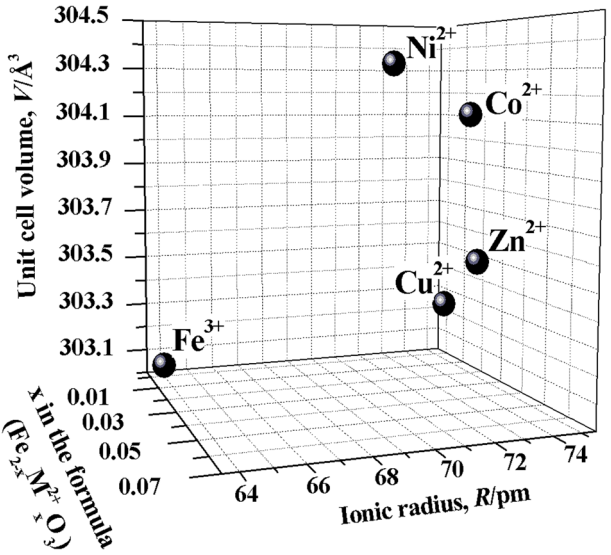


**Fig. 4** Variation of the trigonal hexagonal unit cell volume for the pure and cation-doped hematites as function of the ionic radius in a six-coordinated M-O (M = $Fe^{3+}$; $Cu^{2+}$; $Zn^{2+}$; $Co^{2+}$ or $Ni^{2+}$) chemical environment and the molar proportion (x, in the general formula $\alpha Fe_{2-x}M_xO_3$) of the doping cation

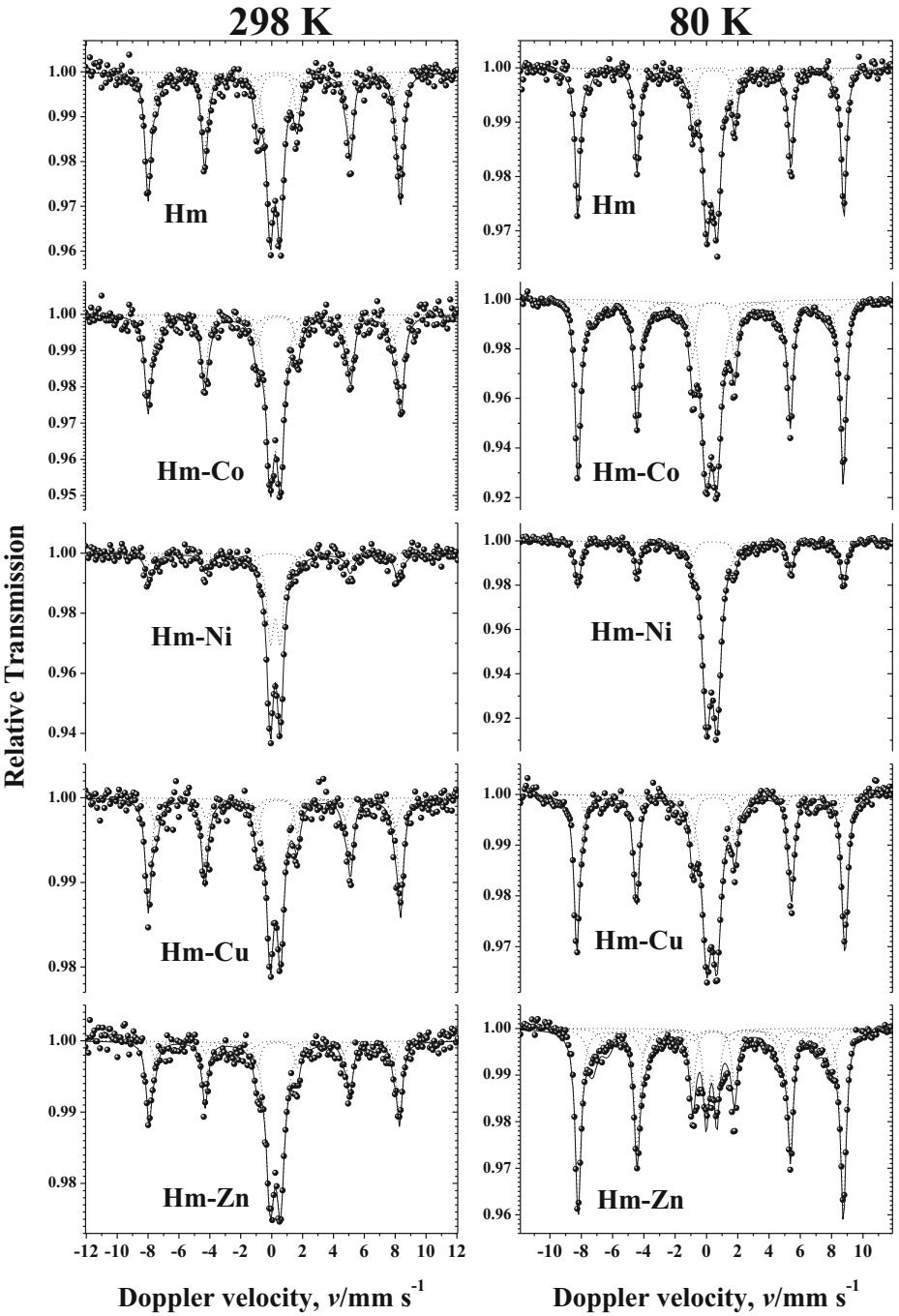


**Fig. 5** $^{57}$Fe Mössbauer spectra recorded at 298 K and 80 K

**Table 1** Parameters from fitting $^{57}$Fe Mössbauer spectra recorded at 298 K

| Sample | Fe site | $\delta$/mm s$^{-1}$ | $2\varepsilon$, $\Delta$/mm s$^{-1}$ | $\Gamma$/mm s$^{-1}$ | $B_{hf}$/T | $RA$/% |
|---|---|---|---|---|---|---|
| Hm | Hm | 0.373(5) | −0.21(1) | 0.46(2)** | 50.64(5) | 52(2) |
| | $Fe^{3+}$ | 0.330(1) | 0.64(1) | 0.56(2) | | 37(1) |
| | Mh | 0.40(3) | 0* | 0.46(2)** | 47.8(2) | 11(1) |
| Hm-Co | Hm | 0.386(7) | −0.20(2) | 0.50(4) | 50.76(8) | 43(4) |
| | $Fe^{3+}$ | 0.337(4) | 0.661(8) | 0.59(2) | | 41(1) |
| | Mh | 0.37(5) | −0.0(2) | 0.6(4) | 47.2(8) | 16(6) |
| Hm-Ni | Hm | 0.39(2) | −0.25(2) | 0.61(7) | 50.0(1) | 29.6(3) |
| | $Fe^{3+}$ | 0.336(4) | 0.645(5) | 0.52(1) | | 70.4(1) |
| Hm-Cu | Hm | 0.383(7) | −0.19(2) | 0.45(3) | 50.66(7) | 45(4) |
| | $Fe^{3+}$ | 0.343(5) | 0.671(9) | 0.55(2) | | 39(1) |
| | Mh | 0.36(3) | 0* | 0.6(1) | 48.0(3) | 16(4) |
| Hm-Zn | Hm | 0.376(8) | −0.20(2) | 0.44(3)** | 50.29(9) | 39(3) |
| | $Fe^{3+}$ | 0.345(4) | 0.66(1) | 0.64(2) | | 52(1) |
| | Mh | 0.30(3) | 0* | 0.44(3)** | 49.9(3) | 9(2) |

$\delta$ = isomer shift relative to $\alpha$Fe; $2\varepsilon$ = quadrupole shift; $\Delta$ = quadrupole splitting; $\Gamma$ = line width; $B_{hf}$ = magnetic hyperfine field; $RA$ = relative subspectral area. The numbers in parentheses are uncertainties over the last significant digit, as a direct output from the least-squares fitting computer program

*Fixed parameter during least-squares fitting convergence

**Constrained parameter during least-squares fitting convergence

bandgap values (1.68, 1.86, 1.77 and 1.75 eV, respectively) were found to be significantly lower than that for the pure hematite.

The variation of the unit cell volume obtained from the refinement of the XRD patterns data for the pure and cation-doped hematites as function of the ionic radius in a six-coordinated M-O (M = $Fe^{3+}$; $Cu^{2+}$; $Zn^{2+}$; $Co^{2+}$ or $Ni^{2+}$) chemical environment and the molar proportion ($x$, in the general formula $\alpha Fe_{2-x}M_xO_3$) of the doping cation is shown in Fig. 4. As expected, it is shown that two elemental characteristics, namely the ionic radius of the divalent cation and its concentration in the solid solution, contribute to vary the unit cell dimension.

The Mössbauer data (spectra in Fig. 5 and corresponding fitted spectral parameters in Tables 1 and 2) confirm that, except for the Ni-doped hematite, spectra at 298 K and 80 K are due to $^{57}$Fe sites corresponding to the typical hyperfine structure of hematite and to a minor proportion of maghemite ($\gamma Fe_2O_3$). The rest of the spectral resonance lines may be interpreted as being due to superparamagnetic $\alpha Fe_{2-x}M_xO_3$ of very small particle sizes (smaller than ∼20 nm, a reasonably representative mean particle size for these samples, as calculated from XRD data using the Scherrer equation) of the iron-bearing species in these samples: part of the subspectral areas of the doublets at 298 K is relatively reduced and those of the sextets is increased, meaning that part of the magnetic relaxation is blocked, on cooling the samples to 80 K. Differently from the other cation-doped samples, the XRD pattern for the Ni-doped hematite shows broader diffraction peaks over a somewhat curved baseline. This is consistent with the relatively more intense doublet of the corresponding 298 K- and 80 K-Mössbauer spectra. These results may mean that very likely the superparamagnetic fraction, due relatively smaller particles, is higher for the Ni- than for the other cation- doped hematite samples.

**Table 2** Parameters from fitting $^{57}$Fe Mössbauer spectra recorded at 80 K

| Sample | Fe site | $\delta$/mm s$^{-1}$ | $2\varepsilon$, $\Delta$/mm s$^{-1}$ | $\Gamma$/mm s$^{-1}$ | $B_{hf}$/T | $RA$/% |
|---|---|---|---|---|---|---|
| Hm | Hm | 0.477(4) | -0.20(1) | 0.39(1)** | 52.73(3) | 55(1) |
| | $Fe^{3+}$ | 0.449(5) | 0.67(1) | 0.59(1) | | 41(1) |
| | Mh | 0.44(5) | 0* | 0.39(1)** | 48.5(4) | 4(1) |
| Hm-Co | Hm | 0.463(1) | −0.192(3) | 0.425(5) | 52.56(1) | 48.8(5) |
| | $Fe^{3+}$ | 0.421(3) | 0.688(5) | 0.725(9) | | 35.2(2) |
| | Mh | 0.46(2) | 0* | 1.26(9) | 46.4(2) | 16(1) |
| Hm-Ni | Hm | 0.477(5) | −0.21(1) | 0.43(2) | 52.62(5) | 28.7(5) |
| | $Fe^{3+}$ | 0.439(2) | 0.665(4) | 0.634(7) | | 71.3(4) |
| Hm-Cu | Hm | 0.482(3) | −0.185(8) | 0.44(1) | 53.14(3) | 56(2) |
| | $Fe^{3+}$ | 0.445(6) | 0.662(8) | 0.68(2) | | 40(1) |
| | Mh | 0.50(3) | 0* | 0.23(9) | 51.0(2) | 4(1) |
| Hm-Zn | Hm | 0.480(2) | −0.191(4) | 0.425(7) | 52.56(2) | 55.9(9) |
| | $Fe^{3+}$ | 0.425(5) | 0.67(1) | 0.40* | | 12.5(2) |
| | Mh | 0.44(1) | 0* | 0.82(5)** | 47.3(1) | 21(1) |
| | Mh | 0.44(3) | 0* | 0.82(5)** | 41.4(2) | 10.6(8) |

$\delta$ = isomer shift relative to $\alpha$Fe; $2\varepsilon$ = quadrupole shift; $\Delta$ = quadrupole splitting; $\Gamma$ = line width; $B_{hf}$ = magnetic hyperfine field; $RA$ = relative subspectral area. The numbers in parentheses are uncertainties over the last significant digit, as a direct output from the least-squares fitting computer program

*Fixed parameter during least-squares fitting convergence

**Constrained parameter during least-squares fitting convergence

The $^{57}$Fe Mössbauer spectroscopy provides an indispensable nuclear probe to experimentally assess the hyperfine structure of the $^{57}$Fe nucleus. However, the atomic proportion of the doping foreign cation, in each of these solid solutions, is very low, and any of such influence promoted by magnetic or electric field to the probe-nucleus would be hardly observed for these samples. Under such circumstances no effect of the doping cation on the $^{57}$Fe hyperfine structure was thus considered.

### 3.2 Photocatalytic activity

The photocatalytic activity of these materials was evaluated by following the decomposition of the indigo carmine dye in water under visible light. Figure 1 shows the optical absorbance spectra at 400-800 nm, for the system resulting from the photochemical degradation of this dye, for all catalyst samples. Results indicate that the photochemical degradation activities are higher for the Cu- and Zn-doped hematites; no significant effect was observed for the Co- and Ni-doped hematites. Bonfim et al. [12] reportedly proposed the catalytic mechanism of the Zn-doped hematite on the dehydrogenation of ethylbenzene. They believe that the zinc ions have a lower electrostatic potential as compared to that of iron ions and then make the lattice less rigid, increasing the mobility of the species to sinter, and this changes the structure of the hematite.

Rocha et al. [13] reported the effect of copper ions on the photocatalytic activity of a semiconductor based on anatase ($TiO_2$) and hematite ($\alpha Fe_2O_3$). Their results showed that the copper dopant tends to increase the degradation activity of the methylene blue dye, and

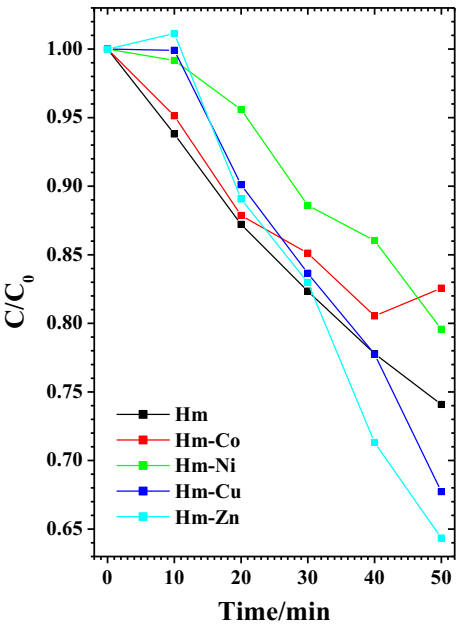


**Fig. 6** Photocatalytic activity of the materials prepared in the degradation of indigo carmine dye

this increase is related to the $Cu^{+}$ and $Cu^{2+}$ species acting as donor centers and electron acceptors, respectively.

From these photocatalytic activity (the data from Fig. 1 were suitably converted to the new representation on coordinates of Fig. 6 in order to emphasize the kinetic trends), a number of factors govern the degradation reaction, namely the ability (i) to absorb light in the visible spectrum and (ii) to increase the mobility of the chemical species. Other reported works have also shown that different semiconductors based on doped-hematite can trap the photo-induced electrons hence alleviating their recombination with the positive holes [14, 15].

## 4 Conclusions

The $Co^{2+}$-, $Ni^{2+}$-, $Cu^{2+}$- or $Zn^{2+}$-doped hematites had their crystallographic unit cell slightly modified, relatively to the pure hematite. The photocatalytic efficiency for both the $Cu^{2+}$- and $Zn^{2+}$-doped hematites on the degradation of the indigo carmine dye was improved, whereas for the $Co^{2+}$- and $Ni^{2+}$-doped hematites the activity was lowered, relatively to the pure hematite. These results for the $Cu^{2+}$- and $Zn^{2+}$-hematite-based semiconductors suggest their real potential as an alternative material to be used on the photocatalytic environmental remediation of water bodies contaminated with organic pollutants.

**Acknowledgements** Work supported by FAPEMIG and CNPq (Brazil; including grant # 305755-2013-7). EJM thanks CAPES (Brazil) for sponsoring her MSc studentship at UFVJM. The authors are indebted to Mr Abraão José Silva Viana and Mr José Joaquim de Sá Teles (UFVJM) for their technical assistance on the EDXRF analysis and collection of the powder X-ray diffraction data and to Mr João Batista Santos Barbosa and Mr Tércio Assunção Pedrosa (CDTN) for their technical assistance on obtaining the powder DRX and SEM-EDS data, respectively. JDF is particularly indebted to CAPES (Brazil) for granting his Visiting Professorship at UFVJM under the PVNS program.

## References


1. Cao, Z., Qin, M., Gu, Y., Jia, B., Chen, P., Qu, X.: Synthesis and characterization of Sn-doped hematite as visible light photocatalyst. Mater. Research Bull. **77**, 41–47 (2016). doi:10.1016/j.materresbull.2016.01.004
2. Wu, Q., Zhao, J., Liu, K., Wang, H., Sun, Z., Li, P., Xue, S.: Ultrathin hematite film for photoelectrochemical water splitting enhanced with reducing graphene oxide. Int. J. Hydrogen Energy **40**, 6763–6770 (2015). doi:10.1016/j.ijhydene.2015.03.160
3. Yang, X., Ma, F., Li, K., Guo, Y., Hu, J., Li, W., Huo, M., Guo, Y.: Mixed phase titania nanocomposite co-doped with metallic silver and vanadium oxide: new efficient photocatalyst for dye degradation. J. Hazard. Mater. **175**, 429–438 (2010). doi:10.1016/j.jhazmat.2009.10.024
4. Tamirat, A.G., Su, W.-N., Dubale, A.A., Pan, C.-J., Chen, H.-M., Ayele, D.W., Lee, J.-F., Hwang, B.-J.: Efficient photoelectrochemical water splitting using three dimensional urchin-like hematite nanostructure modified with reduced graphene oxide. J. Power Sources. **287**, 119–128 (2015). doi:10.1016/j.jpowsour.2015.04.042
5. Lee, C.-Y., Wang, L., Kado, Y., Kirchgeorg, R., Schmuki, P.: Si-doped $Fe_2O_3$ nanotubular/nanoporous layers for enhanced photoelectrochemical water splitting. Electrochem. Communi. **44**, 308–311 (2013). doi:10.1016/j.elecom.2013.07.024
6. Pawar, R.C., Pyo, Y., Ahn, S.H., Lee, C.S.: Photoelectrochemical properties and photodegradation of organic pollutants using hematite hybrids modified by gold nanoparticles and graphitic carbon nitride. Appl. Catal. B Environ. **176-177**, 654–666 (2015). doi:10.1016/j.apcatb.2015.04.045
7. Cornell, R.M., Schwertmann, U.: The Iron Oxides: Structure, Properties, Reactions, Occurrences and Uses. Wiley-VCH Verlag GmbH & Co. KGaA, Weinheim. ISBN 3-527-30274-3 (2003)
8. Scherrer, P., Nachrichten, G. (1918). Apud: Patterson, A.L.: The Scherrer formula for X-ray particle size determination. Phys. Rev. **56**, 978–982 (1939). doi:10.1103/PhysRev.56.978
9. JCPDS–Joint Committee on Powder Diffraction Standards. Mineral Powder Diffraction Files Data Book, Swarthmore, Pennsylvania (1980)
10. Ramasami, A.K., Ravishankar, T.N., Sureshkumar, K., Reddy, M.V., Chowdari, B.V.R., Ramakrishnappa, T., Balakrishna, G.R.: Synthesis, exploration of energy storage and electrochemical sensing properties of hematite nanoparticles. J. Alloys and Compounds. **671**, 552–559 (2016). doi:10.1016/j.jallcom.2016.02.050
11. Phuan, Y.W., Chong, M.N., Egamparan, K., Lee, B.-K., Zhu, T., Chan, E.S.: Understanding the synergistic between optimum dopant loading and charge transfer kinetics in platinum-mediated nanostructured hematite thin films. J. Taiwan Institute Chem. Eng. In Press. doi:10.1016/j.jtice.2016.06.031 (2016)
12. Bomfim, H.E.L., Oliveira, A.C., Rangel, M.C.: Effect of zinc on the catalytic activity oh hematite in ethylbenzene dehydrogenation. React. Kinet. Catal. Lett. **80**, 359–364 (2003). doi:10.1023/B:REAC.0000006146.85916.9d
13. Rocha, V.M.S., Pereira, M.G., Teles, L.R., Souza, M.O.G.: Effect of copper on the photocatalytic activity of semiconductor-based titanium dioxide (anatase) and hematite ($\alpha$-$Fe_2O_3$). Mater. Sci. Eng. B **185**, 13–20 (2014). doi:10.1016/j.mseb.2014.02.004
14. Saremi-Yarahmadi, S., Wijayantha, K.G.U., Tahir, A.A., Vaidhyanathan, B.: Nanostructured $\alpha$-$Fe_2O_3$ electrodes for solar driven water splitting: Effect of doping agents on preparation and performance. J. Phys. Chem. C **113**, 4768–4778 (2009). doi:10.1021/jp808453z
15. Bagwasi, S., Tian, B., Zhang, J., Nasir, M.: Synthesis, characterization and application of bismuth and boron Co-doped $TiO_2$: A visible light active photocatalyst. Chem. Eng. J. **217**, 108–118 (2013). doi:10.1016/j.cej.2012.11.080